Determination of a Key Pandemic Parameter of the SIR-Epidemic Model from Past Covid-19 Mutant Waves and Its Variation for the Validity of the Gaussian Evolution

Reinhard Schlickeiser * and Martin Kröger *

Posted Date: 11 January 2023

doi: 10.20944/preprints202301.0188.v1

Keywords: coronavirus; statistical analysis; extrapolation; parameter estimation; pandemic spreading

Article

Determination of a Key Pandemic Parameter of the SIR-Epidemic Model from Past Covid-19 Mutant Waves and Its Variation for the Validity of the Gaussian Evolution

Reinhard Schlickeiser [1,2,*] and Martin Kröger [3,4,*]

[1] Institut für Theoretische Physik, Lehrstuhl IV: Weltraum- und Astrophysik, Ruhr-Universität Bochum, D-44780 Bochum, Germany; rsch@tp4.rub.de
[2] Institut für Theoretische Physik und Astrophysik, Christian-Albrechts-Universität zu Kiel, Leibnizstr. 15, D-24118 Kiel, Germany
[3] Magnetism and Interface Physics, Department of Materials, ETH Zurich, Zurich CH-8093, Switzerland; mk@mat.ethz.ch
[4] Polymer Physics, Department of Materials, ETH Zurich, Zurich CH-8093, Switzerland
* Correspondence: rsch@tp4.rub.de (R.S.), mk@mat.etz.ch (M.K.)

Abstract: Monitored differential infection rates of past Corona waves are used to infer, a posteriori, the real time variation of the ratio of recovery to infection rate as key parameter of the SIR-epidemic model. From monitored Corona waves in five different countries it is found that this ratio exhibits a linear increase at early times below the first maximum of the differential infection rate before the ratios approach a nearly constant value close to unity at the time of the first maximum with small amplitude oscillations at later times. The observed time dependencies at early times and at times near the first maximum agree favorably well with the behavior of the calculated ratio for the Gaussian temporal evolution of the rate of new infections, although the predicted linear increase of the Gauss ratio at late times is not observed.

Keywords: coronavirus; statistical analysis; extrapolation; parameter estimation; pandemic spreading

1. Introduction

The susceptible-infected-recovered/removed (SIR) pandemics model developed originally by Kermack and McKendrick [1] and refined by Kendall [2] is the simplest, but still realistic compartment model where persons from a considered population are assigned to the three compartments S (susceptible), I (infectious) and R (recovered/removed). The infection ($a(t)$) and recovery ($\mu(t)$) rates then regulate the transition probability between the compartment fractions. Later refinements of the SIR-model such as the SEIR [3–12], SVEIR [13,14], SEIRD [15], SIRD [16–18], SIRS [19,20] and SIRV [21–24] have introduced additional compartments (for reviews see refs. [25–31]). The SIR-epidemic model provides a good explanation for the temporal evolution of Covid-19 waves from different mutants [32–34].

An important key parameter of the SIR pandemics model is the ratio $k(t) = \mu(t)/a(t)$ of the recovery to infection rate. Existing analytical solutions to the SIR equations in the literature have adopted originally stationary values of $\mu(t) = \mu_0$ and $a(t) = a_0$ leading to the Kermack and McKendrick integral solution [1]. Recently [35,36] this integral solution has been generalized to arbitrary time-dependent infection rates $a(t)$ assuming a stationary value of the ratio $k(t) = k_0$ so that the recovery rate has the same time dependence as the infection rate. A further generalization to slowly time-dependent ratios $k(t)$ is also possible [37].

It is the purpose of the present manuscript to investigate for the first time a different approach. Instead of adopting different choices of the time dependence of the key parameter $k(t)$ and then solve the SIR equations as before we follow a different line of argument: in Section 2 we express the ratio $k(t)$

Preprints (www.preprints.org) | NOT PEER-REVIEWED | Posted: 11 January 2023 doi:10.20944/preprints202301.0188.v1

in terms of the observable rate of new infections $\dot{J}(t)$ and its corresponding cumulative fraction $J(t)$. By adopting the earlier considered Gaussian evolution function [38–41] for the rate of new infections $\dot{J}(t)$ we then calculate in Section 3 the corresponding time dependence of the ratio $k(t)$. If this required dependence of $k(t)$ agrees with the determination of the ratio $k(t)$ from monitored infection rates in different pandemic waves (Section 4) it would prove the validity of the Gauss model for the time evolution of pandemic waves.

2. SIR model

2.1. Starting equations

The original SIR-equations read

$$\frac{dS}{dt} = -a(t)SI, \tag{1a}$$

$$\frac{dI}{dt} = a(t)SI - \mu(t)I, \tag{1b}$$

$$\frac{dR}{dt} = \mu(t)I, \tag{1c}$$

obeying the sum constraint

$$S(t) + I(t) + R(t) = 1 \tag{2}$$

at all times $t \geq t_0$ after the start of the wave at time t_0 with the initial consitions [36]

$$I(t_0) = \eta, \quad S(t_0) = 1 - \eta, \quad R(t_0) = 0. \tag{3}$$

where η is positive and usually very small, $\eta \ll 1$. Very accurate analytical approximations [42] of the solutions of the SIR-equations (1)–(2) have been derived recently assuming a stationary value of the ratio $k(t) = a(t)/\mu(t) = k_0$. In Section 4 we also use the monitored data on the temporal evolution of pandemic waves in different countries to test the validity of the stationarity of $k(t)$.

2.2. Key parameter

In terms of the reduced time

$$\tau = \int_{t_0}^{t} d\xi\, a(\xi) \tag{4}$$

the SIR equations (1) read

$$\frac{dS}{d\tau} = -SI, \tag{5a}$$

$$\frac{dI}{d\tau} = SI - k(\tau)I, \tag{5b}$$

$$\frac{dR}{d\tau} = k(\tau)I, \tag{5c}$$

as with the time-dependent ratio

$$k(\tau(t)) = \frac{\mu(t)}{a(t)}. \tag{6}$$

Equation (5a) provides

$$I(\tau) = -\frac{dS(\tau)/d\tau}{S(\tau)} = -\frac{d\ln S(\tau)}{d\tau} = \frac{d}{d\tau}\ln(1 - J(\tau))^{-1} = \frac{j(\tau)}{1 - J(\tau)} \tag{7}$$

Preprints (www.preprints.org) | NOT PEER-REVIEWED | Posted: 11 January 2023 doi:10.20944/preprints202301.0188.v1

in terms of the rate of new infections $j(\tau) = SI = dJ(\tau)/d\tau$ and the cumulative number of new infections $J = \int_0^\tau d\xi j(\xi)$. In deriving Equation (7) we have used that $S(\tau) = 1 - J(\tau)$. Likewise Equation (5b) yields

$$k(\tau) = S - \frac{d\ln I}{d\tau} = 1 - J(\tau) - \frac{d}{d\tau}\ln\left[\frac{d}{d\tau}\ln(1-J(\tau))^{-1}\right], \tag{8}$$

where we inserted Equation (7).

As an aside we note that the same relation (8) results if we use Eqs. (5c)–(7) and the sum constraint (2), i.e.

$$k(\tau) = \frac{dR/d\tau}{I} = \frac{\frac{d}{d\tau}(1-S-I)}{I} = -\left(\frac{d\ln I}{d\tau} + \frac{\frac{dS}{d\tau}}{I}\right) = -\frac{d\ln I}{d\tau} + S, \tag{9}$$

where in the last step we inserted Equation (7).

In terms of the real time $\dot{J}(t) = a(t)j(\tau)$ and $J(t) = J(\tau)$ Equation (8) finally reads

$$k(t) = \frac{\mu(t)}{a(t)} = 1 - J(t) - \frac{1}{a(t)}\frac{d}{dt}\ln\left[\frac{1}{a(t)}\frac{d}{dt}(1-J(t))^{-1}\right] \tag{10}$$

in terms of the monitored cumulative rate of new infections $J(t)$ and the time-dependent infection rate $a(t)$.

Multiplying Equation (10) with $a(t)$ then provides

$$\mu(t) = [1-J(t)]\,a(t) - \frac{d}{dt}\ln\left[\frac{\dot{J}(t)}{a(t)(1-J(t))}\right], \tag{11}$$

and for a stationary infection rate a_0, Eqs. (10)–(11) simplify to

$$\begin{aligned} k(t) &= \frac{\mu(t)}{a_0} = 1 - J(t) - \frac{1}{a_0}\frac{d}{dt}\ln\left[\frac{\dot{J}(t)}{a_0(1-J(t))}\right] \\ &= 1 - J(t) - \frac{1}{a_0}\frac{d}{dt}\ln\left[\frac{1}{a_0}\frac{d}{dt}\ln(1-J(t))^{-1}\right] \\ &= 1 - J(t) - \frac{1}{a_0}\left[\frac{\ddot{J}(t)}{\dot{J}(t)} + \frac{\dot{J}(t)}{1-J(t)}\right] \end{aligned} \tag{12}$$

and

$$\mu(t) = [1-J(t)]a_0 - \frac{d}{dt}\ln\left[\frac{1}{a_0}\frac{d}{dt}\ln(1-J(t))^{-1}\right], \tag{13}$$

respectively. In the case of stationary infection rate the entire real time dependence of the ratio $k(t)$ is attributed to a time-dependent recovery rate $\mu(t)$.

We emphasize that Eqs. (9)–(13) hold for all reduced (τ) and real (t) times.

2.3. Limiting case $J(t) \ll 1$

In practically all Covid-19 mutant waves the final cumulative fraction of infected persons is much less than unity, i.e. $J_\infty \ll 1$. In the limit $J(t) \le J_\infty \ll 1$ we use the approximations

$$1 - J(t) \simeq 1, \quad \ln(1-J(t))^{-1} \simeq J(t), \tag{14}$$

Preprints (www.preprints.org) | NOT PEER-REVIEWED | Posted: 11 January 2023 doi:10.20944/preprints202301.0188.v1

so that Eqs. (10)–(11) reduce to

$$\begin{aligned} k(t) &\simeq 1 - J(t) - \frac{1}{a(t)}\frac{d}{dt}\ln\frac{\dot{J}(t)}{a(t)}, \\ \mu(t) &\simeq [1 - J(t)]a(t) - \frac{d}{dt}\ln\frac{\dot{J}(t)}{a(t)}, \end{aligned} \tag{15}$$

and in case of stationary infection rates

$$\begin{aligned} k(t) &\simeq 1 - J(t) - \frac{1}{a_0}\frac{d}{dt}\ln\frac{\dot{J}(t)}{a_0} = 1 - J(t) - \frac{\ddot{J}(t)}{a_0\dot{J}(t)} \\ &= 1 - J(t) - \frac{1}{a_0}\frac{d\ln\dot{J}(t)}{dt}, \\ \mu(t) &\simeq a_0 - \frac{d}{dt}\ln\dot{J}(t). \end{aligned} \tag{16}$$

The first Equation (16) indicates that a small value of the stationary infection rate a_0 provides a smaller value of the ratio $k(t)$ close to zero.

3. Condition for the validity of the Gaussian evolution

In this Section we adopt the Gaussian evolution for the rate of new infections [40,41]

$$\dot{J}(t) = \frac{J_\infty}{\sqrt{\pi}\Delta}\exp\left[-\frac{(t - t_{\max})^2}{\Delta^2}\right]. \tag{17}$$

The corresponding accumulative fraction of infections at any time then is given by

$$J(t) = \int_{-\infty}^{t} dt'\, e^{-\frac{(t'-t_{\max})^2}{\Delta^2}} = \frac{J_\infty}{2}\left[1 + \mathrm{erf}\left(\frac{t - t_{\max}}{\Delta}\right)\right] \tag{18}$$

in terms of the error function. J_∞ denotes the final cumulative fraction of infections after infinite time $t \to \infty$.

The Gaussian evolution (17) implies

$$\ddot{J}(t) = -\frac{2(t - t_{\max})}{\Delta^2}\dot{J}(t). \tag{19}$$

In the general case of arbitrarily large J_∞ the full Equation (12) yields for the Gauss evolution

$$\begin{aligned} k(t) &= 1 - \frac{J_\infty}{2}\left[1 + \mathrm{erf}\left(\frac{t - t_{\max}}{\Delta}\right)\right] + \frac{2(t - t_{\max})}{a_0\Delta^2} \\ &\quad - \frac{J_\infty e^{-\frac{(t-t_{\max})^2}{\Delta^2}}}{\sqrt{\pi}a_0\Delta\left\{1 - \frac{J_\infty}{2}\left[1 + \mathrm{erf}\left(\frac{t-t_{\max}}{\Delta}\right)\right]\right\}}. \end{aligned} \tag{20}$$

In the limit $J_\infty \ll 1$, as also indicated by the first Equation (16), the last term in Equation (20) is negligibly small providing in this limit

$$k(t) \simeq 1 - \frac{J_\infty}{2}\left[1 + \mathrm{erf}\left(\frac{t - t_{\max}}{\Delta}\right)\right] + \frac{2(t - t_{\max})}{a_0\Delta^2}. \tag{21}$$

The full ratio (20) and its approximation (21) are shown in Figure 1. One notices that the approximation (21) agrees very well with the exact time variation (20). Obviously Figure 1 indicates three different regimes in time for the Gauss ratio:

Preprints (www.preprints.org) | NOT PEER-REVIEWED | Posted: 11 January 2023 doi:10.20944/preprints202301.0188.v1

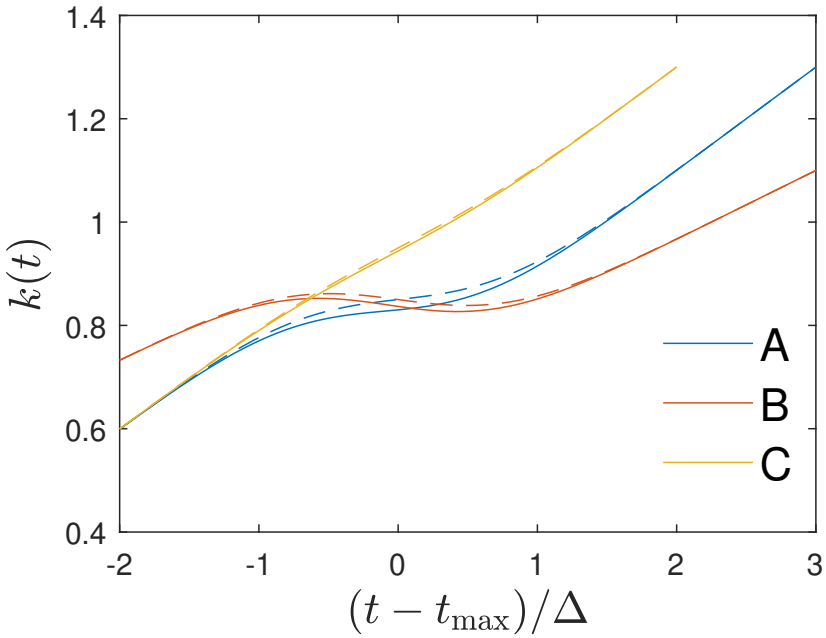

Figure 1. The Gauss ratio (20) (full curves) and its approximation (21) (dashed curves) plotted for the three cases (A) $a_0 = 1$ days^{-1}, $J_\infty = 0.3$, $\Delta = 10$ days, (B) $a_0 = 0.5$ days^{-1}, $J_\infty = 0.3$, $\Delta = 30$ days, and (C) $a_0 = 0.5$ days^{-1}, $J_\infty = 0.1$, $\Delta = 20$ days, respectively.

(i) At *early times* $t \ll t_{\max}$ the Gauss ratio increases linearly starting from ratio values less than unity.
(ii) At *times near maximum*, i.e. close to $t_{\max}$ near the maximum of $\dot{J}(t)$, the Gauss ratio exhibits a dip which is more pronounced for smaller values of a_0 which is also indicated by Equation (21) as the third linear term is inversely proportional to a_0.
(iii) At *late times* beyond $t_{\max}$ the Gauss ratio resumes its linear increase with time.

We conclude that for the time dependency (20) of the ratio $k(t)$ the Gaussian evolution (17) is an exact analytical solution of the SIR equations. Likewise, if the monitored differential and cumulative infection rates $\dot{J}(t)$ and $J(t)$ inserted in Equation (12) are well approximated by the Gaussian ratios (20) and (21) in all three distinct time regimes we can justify the use the Gaussian evolution (17) as good approximations of the solutions of the SIR equations.

4. Determination of the ratio (12) from monitored infection rates of Covid-19 waves

In Figure 2 we show in the left panels the differential infection rate $\dot{J}(t)$ in the five countries Germany, Switzerland, The Netherlands, United States, and Sweden inferred from the reported death rates adopting a fatality rate of 0.005. In each country the raw data (in grey) have been smoothed (black curves) in order to infer the second derivative $\ddot{J}(t)$. More details on the considered Corona waves are given in the caption of Figure 2. The respective right panels show the derived ratio $k(t)$ calculated from Equation (16) for different values of the stationary infection rate a_0.

The monitored infection rates exhibit one clear maximum during the selected time spans capturing a single wave. The corresponding inferred ratios $k(t)$ in these countries remarkably show more or less similar behaviors. In all cases, except Sweden, one notices a linear increase at early times below the first maximum of $\dot{J}(t)$ before the ratios approach a nearly constant value close to unity at the time of the first maximum with small amplitude oscillations at later times. A resumed linear increase of the ratio at late times is not visible. Consequently, we may conclude that the Gaussian evolution (17) provides a good approximation of the solutions of the SIR equations during early and peak times. It however fails at late times beyond the first maximum of the considered past corona waves in these five countries. This good agreement of the Gauss modeling at times prior the maximum in the monitored differential infection rates justifies a posteriori the earlier approaches [38–41]. Moreover, the almost constant

 doi:10.20944/preprints202301.0188.v1

values of the ratio $k(t)$ at times after the maximum time indicates that the analytical SIR-solutions [35,36] based on a constant ratio are well applicable at these times.

Common to all five examples shown in Figure 1 is that only one clear maximum in the differential rate of new infections is visible. In Figure 3 we show the differential rate of new infections on a longer time scales in the United States. Here at least three maxima are exhibited so that the ratio $k(t)$ at late times deviates from its nearly constant value and decreases substantially with time. This clearly demonstrates that a decreasing ratio $k(t)$ to values considerably less than unity is responsible for leading to new maxima in the rate of new infections of the same mutant.

Preprints (www.preprints.org) | NOT PEER-REVIEWED | Posted: 11 January 2023 doi:10.20944/preprints202301.0188.v1

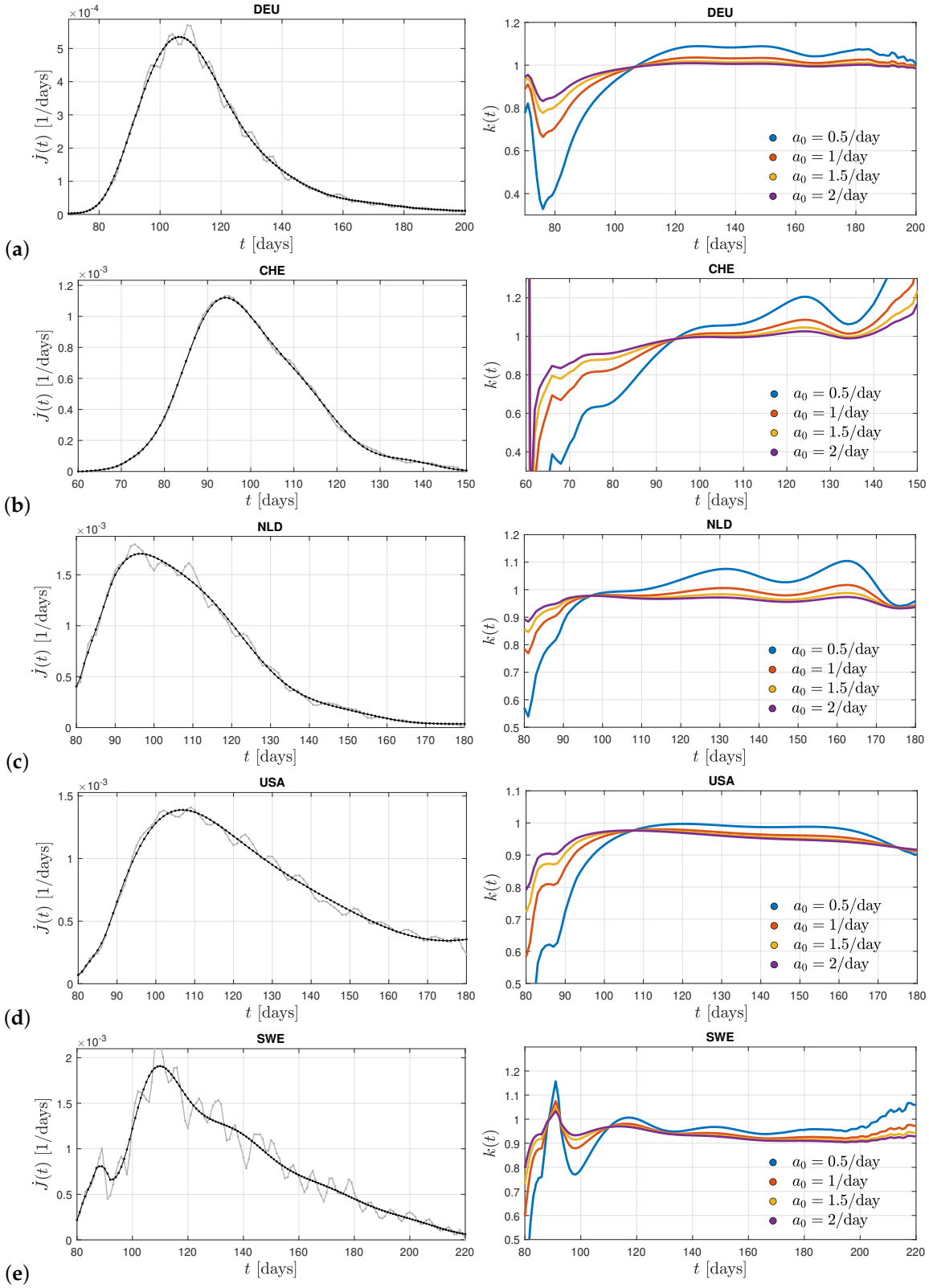

Figure 2. Differential infection rate $\dot{J}(t)$ in (**a**) Germany from the first corona wave during days 70–200 (March 10 - July 18) in the year 2020 inferred from the reported death rates adopting a fatality rate of 0.005 (left panel). The raw data (in grey) are smoothed (black curve) in order to infer the second derivative $\ddot{J}(t)$. The right panel shows the derived ratio $k(t)$ calculated from Equation (16) for different values of the stationary infection rate a_0. (**b**) Switzerland during days 60–150, (**c**) The Netherlands during days 80-180, (**d**) United States during days 80-180, and (**e**) Sweden during days 80-220, where day 1 is 1 Jan 2020 in each case. Real-time data retrieved from [43].

Preprints (www.preprints.org) | NOT PEER-REVIEWED | Posted: 11 January 2023 doi:10.20944/preprints202301.0188.v1

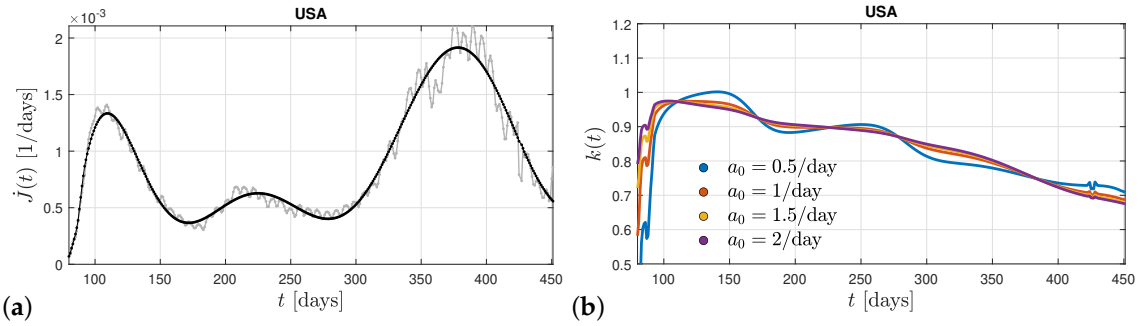

Figure 3. (**a**) Differential infection rate $\dot{J}(t)$ in the United States from the first three corona waves during days 80-450 (20 March 2020 - 24 March 2021) inferred from the reported death rates adopting a fatality rate of 0.005. The raw data (in grey) are smoothed (black curve) in order to infer the second derivative $\ddot{J}(t)$. (**b**) the derived ratio $k(t)$ calculated from Equation (16) for different values of the stationary infection rate a_0. Real-time data retrieved from [43].

5. Summary and conclusions

The SIR-epidemic model provides a good explanation for the temporal evolution of Covid-19 waves from different mutants. An important key parameter of the SIR model is the ratio $k(t) = \mu(t)/a(t)$ of the recovery to infection rate. Here, apparently for the first time, monitored differential infection rates of past Corona waves have been used to infer a posteriori the real time variation of this key parameter. By attributing its time dependence formally to a time dependent recovery rate the temporal evolution of the ratio $k(t)$ is inferred for different values of the stationary infection rate a_0.

For past corona waves in five different countries it is found that the ratio $k(t)$ exhibits a linear increase at early times below the first maximum of the differential infection rate before the ratio approaches a nearly constant value close to unity at the time of the first maximum with small amplitude oscillations at later times.

The observed time dependencies at early times and at times near the first maximum agree favorably well with the behavior of the calculated ratio $k(t)$ for the Gaussian evolution for the rate of new infections, although the predicted linear increase of the Gauss ratio at late times is not observed.

Likewise, the near constancy of the ratio $k(t)$ at times after the maximum time indicates that earlier analytical solutions of the SIR equations for constant ratios are well justified.

On longer time intervals more than one maximum in the differential rate of new infections indicate the presence of several maxima which can be explained by a decrease of the ratio $k(t)$ at times after the first maximum to values considerably less than unity. This decrease then is responsible for causing new maxima in the rate of new infections of the same mutant.

Author Contributions: Conceptualization, R.S.; methodology, R.S., M.K.; software, M.K.; writing—original draft preparation, R.S.; writing—review and editing, R.S., M.K.; visualization, M.K.; All authors have read and agreed to the published version of the manuscript.

Funding: This research received no external funding

Informed Consent Statement: Not applicable.

Data Availability Statement: The raw, real-time data used in this study has been retrieved from [43].

Conflicts of Interest: The authors declare no conflict of interest.

References

1. Kermack, W.O.; McKendrick, A.G. A contribution to the mathematical theory of epidemics. *Proc. R. Soc. A* **1927**, *115*, 700. https://doi.org/10.1098/rspa.1927.0118.
2. Kendall, D.G. Deterministic and stochastic epidemics in closed populations. *Proc. Third Berkeley Symp. on Math. Statist. and Prob.* **1956**, *4*, 149. https://doi.org/10.1525/9780520350717-011.

3. Annas, S.; Pratama, M.I.; Rifandi, M.; Sanusi, W.; Side, S. Stability analysis and numerical simulation of SEIR model for pandemic Covid-19 spread in Indonesia. *Chaos Solit. Fract.* **2020**, *139*, 110072. https://doi.org/10.1016/j.chaos.2020.110072.
4. Hou, C.; Chen, J.; Zhou, Y.; Hua, L.; Yuan, J.; He, S.; Guo, Y.; Zhang, S.; Jia, Q.; Zhao, C.; et al. The effectiveness of quarantine of Wuhan city against the Corona Virus Disease 2019 (Covid-19): A well-mixed SEIR model analysis. *J. Med. Virol.* **2020**, *92*, 841–848. https://doi.org/10.1002/jmv.25827.
5. Yang, Z.; Zeng, Z.; Wang, K.; Wong, S.S.; Liang, W.; Zanin, M.; Liu, P.; Cao, X.; Gao, Z.; Mai, Z.; et al. Modified SEIR and AI prediction of the epidemics trend of Covid-19 in China under public health interventions. *J. Thorac. Dis.* **2020**, *12*, 165+. https://doi.org/10.21037/jtd.2020.02.64.
6. He, S.; Peng, Y.; Sun, K. SEIR modeling of the Covid-19 and its dynamics. *Nonlin. Dyn.* **2020**, *101*, 1667–1680. https://doi.org/10.1007/s11071-020-05743-y.
7. Rezapour, S.; Mohammadi, H.; Samei, M.E. SEIR epidemic model for Covid-19 transmission by Caputo derivative of fractional order. *Adv. Diff. Eqs.* **2020**, *2020*, 490. https://doi.org/10.1186/s13662-020-02952-y.
8. Ghostine, R.; Gharamti, M.; Hassrouny, S.; Hoteit, I. An Extended SEIR Model with Vaccination for Forecasting the Covid-19 Pandemic in Saudi Arabia Using an Ensemble Kalman Filter. *Math.* **2021**, *9*, 636. https://doi.org/10.3390/math9060636.
9. Berger, D.; Herkenhoff, K.; Huang, C.; Mongey, S. Testing and reopening in an SEIR model. *Rev. Econ. Dyn.* **2022**, *43*, 1–21. https://doi.org/10.1016/j.red.2020.11.003.
10. Engbert, R.; Rabe, M.M.; Kliegl, R.; Reich, S. Sequential Data Assimilation of the Stochastic SEIR Epidemic Model for Regional Covid-19 Dynamics. *Bull. Math. Biol.* **2021**, *83*, 1. https://doi.org/10.1007/s11538-020-00834-8.
11. Bentout, S.; Chen, Y.; Djilali, S. Global Dynamics of an SEIR Model with Two Age Structures and a Nonlinear Incidence. *Acta Appl. Math.* **2021**, *171*, 7. https://doi.org/10.1007/s10440-020-00369-z.
12. Carcione, J.M.; Santos, J.E.; Bagaini, C.; Ba, J. A Simulation of a Covid-19 Epidemic Based on a Deterministic SEIR Model. *Front. Publ. Health* **2020**, *8*, 230. https://doi.org/10.3389/fpubh.2020.00230.
13. Nabti, A.; Ghanbari, B. Global stability analysis of a fractional SVEIR epidemic model. *Math. Meth. Appl. Sci.* **2021**, *44*, 8577–8597. https://doi.org/10.1002/mma.7285.
14. Lopez, L.; Rodo, X. A modified SEIR model to predict the Covid-19 outbreak in Spain and Italy: Simulating control scenarios and multi-scale epidemics. *Results Phys.* **2021**, *21*, 103746. https://doi.org/10.1016/j.rinp.2020.103746.
15. Korolev, I. Identification and estimation of the SEIRD epidemic model for Covid-19. *J. Econom.* **2021**, *220*, 63–85. https://doi.org/10.1016/j.jeconom.2020.07.038.
16. Jahanshahi, H.; Munoz-Pacheco, J.M.; Bekiros, S.; Alotaibi, N.D. A fractional-order SIRD model with time-dependent memory indexes for encompassing the multi-fractional characteristics of the Covid-19. *Chaos Solit. Fract.* **2021**, *143*, 110632. https://doi.org/10.1016/j.chaos.2020.110632.
17. Nisar, K.S.; Ahmad, S.; Ullah, A.; Shah, K.; Alrabaiah, H.; Arfan, M. Mathematical analysis of SIRD model of Covid-19 with Caputo fractional derivative based on real data. *Results Phys.* **2021**, *21*, 103772. https://doi.org/10.1016/j.rinp.2020.103772.
18. Faruk, O.; Kar, S. A Data Driven Analysis and Forecast of Covid-19 Dynamics during the Third Wave Using SIRD Model in Bangladesh. *Covid* **2021**, *1*, 503–517. https://doi.org/10.3390/covid1020043.
19. Rajasekar, S.P.; Pitchaimani, M. Ergodic stationary distribution and extinction of a stochastic SIRS epidemic model with logistic growth and nonlinear incidence. *Appl. Math. Comput.* **2020**, *377*, 125143. https://doi.org/10.1016/j.amc.2020.125143.
20. Hu, H.; Yuan, X.; Huang, L.; Huang, C. Global dynamics of an SIRS model with demographics and transfer from infectious to susceptible on heterogeneous networks. *Math. Biosci. Eng.* **2019**, *16*, 5729–5749. https://doi.org/10.3934/mbe.2019286.
21. Babaei, N.A.; Ozer, T. On exact integrability of a Covid-19 model: SIRV. *Math. Meth. Appl. Sci.* **2023**. https://doi.org/10.1002/mma.8874.
22. Rifhat, R.; Teng, Z.; Wang, C. Extinction and persistence of a stochastic SIRV epidemic model with nonlinear incidence rate. *Adv. Diff. Eqs.* **2021**, *2021*, 200. https://doi.org/10.1186/s13662-021-03347-3.
23. Ameen, I.; Baleanu, D.; Ali, H.M. An efficient algorithm for solving the fractional optimal control of SIRV epidemic model with a combination of vaccination and treatment. *Chaos Solit. Fract.* **2020**, *137*, 109892. https://doi.org/10.1016/j.chaos.2020.109892.

24. Oke, M.O.; Ogunmiloro, O.M.; Akinwumi, C.T.; Raji, R.A. Mathematical Modeling and Stability Analysis of a SIRV Epidemic Model with Non-linear Force of Infection and Treatment. *Commun. Math. Appl.* **2019**, *10*, 717–731. https://doi.org/10.26713/cma.v10i4.1172.
25. Keeling, M.J.; Rohani, P. *Modeling Infectious Diseases in Humans and Animals*; Princeton University Press, Princeton, USA, 2008. https://doi.org/10.2307/j.ctvcm4gk0.
26. E., E. Covid-19 and Sars-Cov-2, Modeling the present, looking at the future. *Phys. Rep.* **2020**, *869*, 1. https://doi.org/10.1016/j.physrep.2020.07.005.
27. Lopez, L.; Rodo, X. The end of social confinement and Covid-19 re-emergence risk. *Nat. Human Behav.* **2020**, *4*, 746+. https://doi.org/10.1038/s41562-020-0908-8.
28. Miller, I.F.; Becker, A.D.; Grenfell, B.T.; Metcalf, C.J.E. Disease and healthcare burden of Covid-19 in the United States. *Nat. Med.* **2020**, *26*, 1212+. https://doi.org/10.1038/s41591-020-0952-y.
29. Reiner, Jr., R.C.; Barber, R.M.; Collins, J.K.; Zheng, P.; Adolph, C.; Albright, J.; Antony, C.M.; Aravkin, A.Y.; Bachmeier, S.D.; Bang-Jensen, B.; et al. Modeling Covid-19 scenarios for the United States. *Nat. Med.* **2021**, *27*, 94+. https://doi.org/10.1038/s41591-020-1132-9.
30. Linka, K.; Peirlinck, M.; Sahli Costabal, F.; Kuhl, E. Outbreak dynamics of Covid-19 in Europe and the effect of travel restrictions. *Comp. Meth. Biomech. Biomed. Eng.* **2020**, *23*, 710–717. https://doi.org/10.1080/10255842.2020.1759560.
31. Filindassi, V.; Pedrini, C.; Sabadini, C.; Duradoni, M.; Guazzini, A. Impact of Covid-19 First Wave on Psychological and Psychosocial Dimensions: A Systematic Review. *Covid* **2022**, *2*, 273–340. https://doi.org/10.3390/covid2030022.
32. Postnikov, E.B. Estimation of Covid-19 dynamics "on a back-of-envelope?: Does the simplest SIR model provide quantitative parameters and predictions? *Chaos Solit. Fract.* **2020**, *135*, 109841. https://doi.org/10.1016/j.chaos.2020.109841.
33. Cooper, I.; Mondal, A.; Antonopoulos, C.G. A SIR model assumption for the spread of Covid-19 in different communities. *Chaos Solit. Fract.* **2020**, *139*. https://doi.org/10.1016/j.chaos.2020.110057.
34. Hespanha, J.P.; Chinchilla, R.; Costa, R.R.; Erdal, M.K.; Yang, G. Forecasting Covid-19 cases based on a parameter-varying stochastic SIR model. *Annu. Rev. Control* **2021**, *51*, 460–476. https://doi.org/10.1016/j.arcontrol.2021.03.008.
35. Kröger, M.; Schlickeiser, R. Analytical solution of the SIR-model for the temporal evolution of epidemics. Part A: Time-independent reproduction factor. *J. Phys. A* **2020**, *53*, 505601. https://doi.org/10.1088/1751-8121/abc65d.
36. Schlickeiser, R.; Kröger, M. Analytical solution of the SIR-model for the temporal evolution of epidemics: Part B. Semi-time case. *J. Phys. A* **2021**, *54*, 175601. https://doi.org/10.1088/1751-8121/abed66.
37. Kröger, M.; Schlickeiser, R. SIR-solution for slowly time-dependent ratio between recovery and infection rates. *Physics* **2022**, *4*, 504. https://doi.org/10.3390/physics4020034.
38. Ciufolini, I.; Paolozzi, A. Mathematical prediction of the time evolution of the Covid-19 pandemic in Italy by a Gauss error function and Monte Carlo simulations. *Eur. Phys. J. Plus* **2020**, *135*, 355. https://doi.org/10.3390/physics4020034.
39. Lixiang, L.; Yang, Z.; Deng, Z.; Meng, C.; Huang, J.; Meng, H.; Wang, D.; Chen, G.; Zhang, J.; Peng, J. Propagation analysis and prediction of the Covid-19. *Infect. Disease Model.* **2020**, *5*, 282. https://doi.org/10.1016/j.idm.2020.03.002.
40. Schlickeiser, R.; Schlickeiser, F. A gaussian model for the time development of the Sars-Cov-2 corona pandemic disease. Prrdictions for Germany made on March 30. *Physics* **2020**, *2*, 164. https://doi.org/10.3390/physics2020010.
41. Schüttler, J.; Schlickeiser, R.; Schlickeiser, F.; Kröger, M. Covid-19 predictions using a Gauss model, based on data from April 2. *Physics* **2020**, *2*, 197. https://doi.org/10.3390/physics2020013.
42. Kröger, M.; Schlickeiser, R. Verification of the accuracy of the SIR model in forecasting based on the improved SIR model with a constant ratio of recovery to infection rate by comparing with monitored second wave data. *R. Soc. Open Sci.* **2021**, *8*, 211379. https://doi.org/10.1098/rsos.211379.
43. Dong, E.; Du, H.; Gardner, L. An interactive web-based dashboard to track Covid-19 in real time. *Lancet* **2020**, *5*, 533–534. https://pomber.github.io/covid19/timeseries.json.

 doi:10.20944/preprints202301.0188.v1